Title

Dissecting effects of prodromal intestinal inflammation on the neurodegeneration and neuroinflammation in a Parkinson's disease model

Permalink

https://escholarship.org/uc/item/94r042wr

Author

Espey, Hannah

Publication Date

2022

Peer reviewed|Thesis/dissertation

UNIVERSITY OF CALIFORNIA

Los Angeles

Dissecting effects of prodromal intestinal inflammation on the neurodegeneration and

neuroinflammation in a Parkinson's disease model

A thesis submitted in partial satisfaction of the requirements for the degree

Master of Science in Physiological Science

by

Hannah Ting Espey

2022

ABSTRACT OF THE THESIS

Dissecting effects of prodromal intestinal inflammation on the neurodegeneration and

neuroinflammation in a Parkinson's disease model

by

Hannah Ting Espey

Master of Science in Physiological Science

University of California, Los Angeles, 2022

Professor Elaine Yih-Nien Hsiao, Chair

While Parkinson's disease (PD) is a motor symptom disorder due to neurodegeneration

of dopaminergic neurons and accumulation of Lewy bodies in the substantia nigra (SN),

gastrointestinal dysfunctions are characteristic of prodromal PD. The most common monogenic

mutation for PD lies in the gene leucine rich repeat kinase 2 (LRRK2), which harbors a mutation

associated with IBD within the same locus.

By studying the PD-causing mutation LRRK2 G2019S in transgenic (Tg) mice, we

examined the effect that dextran sulfate sodium (DSS)-induced gut inflammation may have on

the neuropathology of PD. This includes dopaminergic neuron loss, microglial and lysosomal

activation, and alpha-synuclein (αSyn) aggregations in the SN.

We found prodromal DSS-induced colitis exacerbates and accelerates

neurodegeneration in LRRK2 G2019S Tg mice by 52 weeks of age. Prodromal colitis also

promotes microglial activation and lysosomal formation. Interestingly, 23-week-old males

showed increased αSyn aggregations in their microglia. Our data suggests that prodromal gut

inflammation exacerbates the severity and onset of neurodegeneration and promotes

neuroinflammation of PD driven by the LRRK2 G2019S mutation.

The thesis of Hannah Ting Espey is approved.

Arthur P. Arnold

Jonathan P. Jacobs

Elaine Yih-Nien Hsiao, Committee Chair

University of California, Los Angeles

2022

TABLE OF CONTENTS

LIST OF FIGURES

ACKNOWLEDGMENTS

I would like to express my utmost gratitude to Dr. Elaine Hsiao for her support, guidance, and ability to foster such a warm and welcoming lab space. Additionally, I would like to thank Dr. Ping Fang for her mentorship and direct guidance and the entire Hsiao lab for their encouragement. Finally, I would like to acknowledge that my work would not be possible without the collaboration of Dr. Ping Fang, whose own research is referenced in this thesis and is currently in preparation for publication.

Introduction

        Parkinson's disease (PD) is the 2nd most common neurodegenerative disorder afflicting

an estimated 2-3% of the population ≥65 years of age, resulting in motor deficits such as

bradykinesia, rigidity, and tremor (Poewe, et al., 2017; Marras, et al., 2018; Van Den Eeden, et

al., 2003). There are available therapies such as dopamine substitution and deep brain

stimulation to alleviate some symptoms, but treatments to slow or stop the progression of PD

have failed thus far, pushing researchers to explore the mechanistic relationships between early

symptoms and the disease's onset. PD is a motor symptom disorder characterized by the

degeneration of dopaminergic neurons and accumulation of Lewy bodies in the substantia nigra

(SN) that lead to alpha-synuclein (αSyn) aggregations, which is accompanied by inflammatory

microglia and lysosomes that normally engulf and degrade αSyn (Poewe, et al., 2017). While

PD is recognized by its motor deficits, gastrointestinal dysfunctions are a common symptom of

prodromal PD, up to 20 years before the disease is diagnosed (Poewe, et al., 2017).

Furthermore, patients with inflammatory bowel disease (IBD) have been reported to have a

higher risk of PD (Lee, Lobbestael, Vermeire, Sabino, & Cleynen, 2021; Peter, et al., 2018;

Villumsen, Aznar, Pakkenberg, Jess, & Brudek, 2019; Weimers, et al., 2016). Moreover, IBD

patients who were treated with anti-tumor necrosis factor (TNF)α medication, an anti-

inflammatory drug seeking to alleviate IBD symptoms, showed a reduced incidence of PD

compared to patients who did not receive treatment (Peter, et al., 2018), further highlighting a

potential relationship between the diseases.

        A link has been discovered in the gene leucine rich repeat kinase 2 (LRRK2), wherein

mutations within the same locus have been associated with both PD and IBD (Lee, Lobbestael,

Vermeire, Sabino, & Cleynen, 2021). These findings raise the important question of how the PD

mutation LRRK2 G2019S may influence susceptibility to IBD and how the incidence of IBD

could impact the manifestation of PD. Understanding the relationships between genetic risk for

PD and gut inflammation could reveal new molecular targets that inform the development of early interventions that are more effective for treating PD.

Most PD cases are idiopathic, but 15% are known to have genetic underpinnings. The most common monogenic cause for late-onset PD is the autosomal dominant LRRK2 G2019S mutation. This mutation induces hyperactivity of LRRK2 kinase, which leads to hyperphosphorylation of Rab proteins and impaired autophagy and lysosomal formation (Hui, et al., 2018; Alessi & Sammler, 2018; Takagawa, et al., 2018). Cellular models integrating the LRRK2 G2019S mutation show defects in lysosomal activity and deficient clearance of αSyn, which promotes its pathogenic aggregation (Obergasteiger, et al., 2020; Hu, et al., 2018). While the causal mechanism of LRRK2 G2019S mutation is unknown, transgenic mice harboring the human LRRK2 G2019S transgene exhibit progressive aging-dependent development of PD pathology, including αSyn aggregation in the SN and degeneration of dopaminergic neurons (Xiong, et al., 2018). These studies implicate the LRRK2 G2019S mutation as an efficient mouse model of PD.

Furthermore, mutations within the LRRK2 locus suggest a link between IBD and PD. The LRRK2 G2019S mutation has been reported to increase the risk of Crohn's disease (CD) in specific populations (Lee, Lobbestael, Vermeire, Sabino, & Cleynen, 2021). Other LRRK2 mutations, such as the N2081D mutation, have similarly been involved with increased risk of PD and CD, but less strongly associated with PD.

Associations of gut inflammation with the LRRK2 gene can be modeled in mice via experimental gut inflammation induced by sulfated polysaccharide dextran sulfate sodium (DSS). DSS administration is the most widely used method to induce experimental colitis, a common form of IBD, due to its ability to cause intestinal inflammation in the colon and pathology analogous to that seen in ulcerative colitis. Further evidence of association between gut inflammation and the LRRK2 gene was seen in mice overexpressing LRRK2, which were more sensitive to DSS treatment (Takagawa, et al., 2018). However, the biological

consequences of LRRK2 mutations that induce hyperactivity in the kinase domain are unknown in IBD.

DSS-induced gut inflammation has been seen to influence the manifestation in PD of other mouse models. One recent study evaluated effects of DSS-induced gut inflammation in αSyn Tg mice, finding that 92-week-old mice exhibited more substantial loss of dopaminergic neurons in the SN at 18 months post recovery from DSS colitis (Grathwohl, et al., 2021). In another study, wildtype mice exposed acutely to DSS colitis exhibited increased activation of microglia in the hippocampus, suggesting that intestinal inflammation can cause neuroinflammation (Carloni, et al., 2021). These prior data support the hypothesis that DSS-induced gut inflammation promotes neurodegeneration and general neuroinflammation in the brain. However, these effects have not yet been observed specifically in the SN within the LRRK2 G2019S mouse model, which exhibits high face and construct validity for PD.

Based on these previous studies implicating LRRK2 mutations in PD and IBD, and associating risk for IBD with increased risk for PD, we first asked i) does the LRRK2 G2019S mutation for PD increase susceptibility to prodromal intestinal inflammation, and ii) how does prodromal intestinal inflammation influence the severity and onset of PD driven by the LRRK2 G2019S mutation? My research will test the hypothesis that the LRRK2 G2019S mutation increases susceptibility to intestinal inflammation and that early chronic gut inflammation exacerbates or expediates PD neuropathology. Results from my study have the potential to reveal important causal interactions between genetic risk for PD, intestinal inflammation, and brain pathology. Because there are cross-cutting features seen in PD and in other neurodegenerative diseases, findings from my research on the influences of gut inflammation on PD neuropathology could further inform research on gut-brain and neuroimmune contributions to Alzheimer's disease or amyotrophic lateral sclerosis.

Materials and Methods

Mouse genotypes and maintenance

Male and female transgenic (Tg) mice expressing LRRK2^{G2019S} and wildtype (WT) mice on a C57BL/6 background were aged until 23 weeks or 52 weeks. All mice were maintained with same sex littermates, or otherwise singly housed, and kept at a constant temperature with maintained light/dark cycle. They were fed on standard rodent chow and water *ad libitum*. 52-week-old mice: n=5 water-treated LRRK2 G2019S and WT mice, n=5 DSS-treated male and female LRRK2 G2019S mice, n=4 DSS-treated WT female, n=6 DSS-treated WT males. 23-week-old mice: n=5 water-treated and DSS-treated LRRK2 G2019S mice.

DSS-induced gut inflammation

Gut inflammation was induced in 9–13-week-old mice with 2% dextran sodium sulfate (DSS) dissolved in water and provided *ad libitum*. In each round of DSS treatment, mice were treated for seven consecutive days followed by normal water for another seven days. The mice then had a seven-day recovery period, after which another seven days of treatment began until three rounds of DSS treatment had been completed. Body weight was measured, and fecal quality was examined for stool consistency and bleeding to evaluate the severity of gut inflammation induced by DSS treatment. A scoring system was utilized to convert weight loss and stool quality into a clinical score that reflects the effect of DSS-induced chronic gut inflammation. Body weight change, stool consistency, and stool bleeding were given a score 0-4, where 4 reflects exaggerated symptoms. Combined individual scores make up the overall clinical score of the animal per day of treatment. Control groups included age-matched male and female LRRK2^{G2019S} and WT water treated mice.

Histology and Immunohistochemistry

Mice were deeply anesthetized by inhalation of isoflurane, and then transcardially perfused with phosphate-buffered saline (PBS) and 4% paraformaldehyde (PFA) using a micropump. Brains were dissected and post-fixed in 4% PFA for 24 hours before embedding in optimal cutting temperature compound (OCT) and frozen in -80°C.

Standard cryostat procedures were used to cut brains in 25μm thick coronal sections targeting the SN and striatum and collected in PBS. Brain sections were then immunolabeled using standard free-floating techniques by incubating with antibodies for tyrosine hydroxylase (TH), ionized calcium binding adapter molecule 1 (IBA-1), CD68, and α-syn for later visualization of dopaminergic neurons, microglia, lysosomes, and α-synuclein (α-syn) aggregations, respectively. Samples were then incubated with suitable fluorophore-conjugated secondary antibodies in 5% donkey serum. Nuclei were stained with DAPI using slide mounting medium.

Primary antibodies used: TH: AvesLabs, THY, Chicken anti-mouse/hu/ra, 1:500. IBA-1: Fujifilm Wako Chemicals, 019-1974, Rabbit anti-mouse, 1:1000. IBA-1: Fujifilm Wako Chemicals, 011-27991, Goat anti-mouse, 1:1000. CD68 Bio-Rad, MCA1957T, Rat anti-mouse, 1:400. α-syn: Novus Biologicals, NBP2-61121, Rabbit anti-mouse, 1:500.

Secondary antibodies used: Alexa Fluor® 488 AffiniPure Donkey Anti-Rabbit (711-545-152) 1:1000. Alexa Fluor® 594 AffiniPure Donkey Anti-Rat (712-585-153) 1:1000. Alexa Fluor® 647 AffiniPure Donkey Anti-Goat (705-605-003) 1:1000. Alexa Fluor® 647 AffiniPure Donkey Anti-Chicken (703-605-155) 1:1000. DAPI: ThermoFisher, P36962, ProLong™ Diamond Antifade Mountant with DAPI.

Confocal Imaging and Image Analysis

Confocal laser scan microscopy was utilized to acquire images of substantia nigra (SN) of mouse brains using Zeiss confocal (LSM 700, 20x magnification) microscope and Zen Black

software. Only brains with well-defined TH-positive neurons in SN, as well as uniform SN

(Papathanou, et al., 2018; Thompson, Barraud, Andersson, Kirik, & Björklund, 2005; Paul, et al.,

2018), were imaged so each animal had 3-5 imaged sections for counting and analysis. Using

Fiji imaging software, SN area (Papathanou, et al., 2018; Thompson, Barraud, Andersson, Kirik,

& Björklund, 2005; Paul, et al., 2018) was outlined, and subsequent image analysis was

performed in the defined SN area. Average area of SN was 0.94 mm^2 for 52-week-old mice

(average per genotype and sex of 52-week-old mice: LRRK2 G2019S females = 1.04 mm^2,

LRRK2 G2019S males = 0.91 mm^2, WT females = 0.90 mm^2, WT males = 0.89 mm^2) and 0.93

mm^2 for 23-week-old mice (averages per genotype and sex of 23-week-old mice: LRRK2

G2019S females = 0.95 mm^2, LRRK2 G2019S males = 0.90 mm^2).

TH-positive cells were manually counted, ensuring that DAPI signal overlays with the

neuron cell body. Neuron counts were then normalized by SN area to generate neuron density.

IBA-1 positive cells and CD68-positive or αSyn-positive cells that were overlapping with IBA-1

positive cells were manually counted in the SN area to show the amount of activated microglia

with and without lysosomal formation. Only cells with clear IBA-1 signal, microglia morphology,

and DAPI overlay were counted. Positive CD68 signal in the SN was only quantified when within

the IBA-1 signal as puncta, signifying lysosomal formation within the microglia. Similarly,

positive αSyn signal in the microglia was only quantified puncta were present within the

microglia. All manual quantifications of IBA-1 positive-cells, positive-CD68 and αSyn puncta

within IBA-1 were normalized by SN area.

Mean fluorescence intensity (MFI) of IBA-1 and CD68-positive signals in the SN area

was calculated to show extent of microglia activation and lysosomal formation. Positive IBA-1

fluorescent signals in the SN were selected and quantified, and the background fluorescence of

the image subtracted to target only fluorescent signals of IBA-1. Background fluorescence was

subtracted to target only fluorescent signals of CD68. Quantifications were normalized by tissue

area to account for varying SN size. Similarly, MFI of αSyn within the SN and αSyn within the

IBA-1 signal was calculated to show the extent of αSyn presence in the entire SN area or when engulfed by microglia, respectively.

Statistical Analysis

Statistical analysis was performed using GraphPad Prism. Significance was determined by two-way ANOVA, followed by Tukey's post hoc test for multiple group comparisons. Comparisons included interaction analyses of effect of genotype and treatment and genotype and sex on brain pathology (TH-positive neurons, IBA-1 signal, CD68 signal, and αSyn signal). All data are represented as mean ± s.e.m. (standard error of the mean). $*P < 0.05$ was considered statistically significant. $**P < 0.01$. $***P < 0.001$. Notable non-significant (and non-near significant) differences are indicated in the figures by "n.s.".

Results

LRRK2 G2019S mutation increases susceptibility to prodromal intestinal inflammation

We used DSS to induce chronic intestinal inflammation at an early presymptomatic time point in the LRRK2 G2019S mouse model. To mimic an early prodromal IBD, we treated 10–13-week-old LRRK2 G2019S mice with three rounds of 2% DSS dissolved in drinking water, with each round consisting of seven days of DSS treatment followed by seven days of normal drinking water and a seven-day recovery period before beginning the next round **(Fig. 1a)**. Over each treatment period, we measured body weight, where reductions in body weight are a common outcome measure that correlates with severity of intestinal inflammation. We also evaluated stool quality for signs and severity of bleeding and diarrhea, which are characteristic signs of gut inflammation. I used the scoring system developed by Wirtz et al. to convert weight loss and stool quality into a clinical score that reflects the effect of DSS-induced chronic gut inflammation (Wirtz, et al., 2017). Indeed, we observed that DSS induced weight loss and abnormal fecal quality in both male (M) and female (F) wildtype (WT) mice, as expected, demonstrating the effectiveness of this method on inducing gut inflammation **(Fig. 1b, 1c)**. Interestingly, both male and female LRRK2 G2019S mice exhibited exacerbated body weight loss in response to acute intestinal inflammation due to DSS treatment. This was seen only in the first round of DSS treatment; by the third round, there was no significant difference between groups. This suggests that LRRK2 G2019S causes increased susceptibility to acute intestinal inflammation, likely mediated by alterations in innate immune responses.

Dopaminergic neurodegeneration in SN is exacerbated by DSS-induced gut inflammation

To investigate the effects of gut inflammation on neurodegeneration, the SN area of male and female WT and LRRK2 G2019S mice aged 52 weeks was examined for PD-related dopaminergic neuron loss. TH-labeled dopaminergic neurons per area of SN were manually counted to assess neurodegeneration in DSS- and water-treated mouse groups **(Fig. 2)**. DSS-

treated LRRK2 G2019S mice had increased neurodegeneration compared to DSS-treated WT, as seen through decreased TH-positive neuronal density in the SN **(Fig. 2b)**. This demonstrates a genotypic effect where LRRK2 G2019S shows increased neurodegeneration compared to WT with induced gut inflammation. Water-treated WT and LRRK2 G2019S mice showed no difference in dopaminergic neuron density **(Fig. 2b)**, implicating DSS-induced gut inflammation as the main driver for observed neurodegeneration in the SN. Comparing DSS- and water-treated LRRK2 G2019S mice confirm this hypothesis; LRRK2 G2019S mice treated with DSS had increased neurodegeneration compared to those treated with water. Interestingly, DSS-treated LRRK2 G2019S males showed an increase in neurodegeneration compared with DSS-treated WT males, whereas females showed no significant differences **(Fig. 2c)**. These data suggests that gut inflammation affects PD-related neurodegeneration of males more severely than females. Altogether, the dopaminergic neurodegeneration results reveal that DSS colitis exacerbates dopaminergic neurodegeneration in the LRRK2 G2019S mouse model.

Microglial activation and lysosome-positive microglia in SN are increased by DSS-induced gut inflammation in LRRK2 G2019S mice

To investigate the effects of gut inflammation on neuroinflammation, microglia activation and lysosomal formation within microglia were examined for PD-related increases in neuroinflammation. Microglia activation was measured using mean fluorescent intensity (MFI) of the IBA-1 signal, where a more intense fluorescent signal demonstrates an increase in microglial activation **(Fig. 3)**. DSS-treated animals showed increased MFI of IBA-1 in the SN area for both WT and LRRK2 G2019S when compared with their respective water-treated groups **(Fig. 3b)**. DSS-treated mice show an increase in recruited microglia in both WT and LRRK2 G2019S when compared to their water-treated cohort **(Fig. 3c)**. No sex differences were reported when comparing the genotypes within the same sex between and within treatments.

These results suggest that DSS-induced gut inflammation increases microglial activation in the SN area.

Furthermore, lysosomal formation was measured using MFI of the CD68 signal when present within the microglia, where a more intense fluorescent signal demonstrates an increase in lysosomal formation **(Fig. 4a, 4b)**. DSS-treated LRRK2 G2019S mice showed increased MFI of CD68 in the SN area when compared with water-treated LRRK2 G2019S mice, suggesting that DSS colitis increases lysosomal formation within the microglia of LRRK2 G2019S mice.

Microglia and lysosomal MFI were correlated, indicating that as microglia activation increased, lysosomal formation increased **(Fig. 4c)**. To assess if this was due to an overall increase in microglia number or if it was due to an increase of lysosomal formation per microglia, microglia with a positive lysosome signal was manually counted **(Fig. 4a, 4d)**. DSS-treated mice show an increase in CD68-positive microglia in both WT and LRRK2 G2019S when compared to their water-treated cohort, mirroring the increases of microglia **(Fig. 3c)**. No sex differences were reported when comparing the genotypes within the same sex between and within treatments. This data tells that there is an overall increase of lysosome positive microglia, possibly to attempt to clear PD-related αSyn aggregations.

By analyzing microglia activation and lysosome formation in water- and DSS-treated LRRK2 G2019S and WT mice, gut inflammation was found to increase both. This indicates that PD-related neuroinflammation is exacerbated with DSS-induced gut inflammation as evidenced by the increased amount of lysosomal-positive microglia and fluorescent intensities of microglia and lysosomal markers.

Prodromal intestinal inflammation exacerbates onset of PD-related neuroinflammation in males

By investigating αSyn in the SN area, another aspect of severity of PD neuropathology can be observed. Our colleague's work assessing αSyn aggregation in the 52-week-old mice showed that DSS-treated LRRK2 G2019S males have the highest αSyn deposits compared to

WT males, while there is no significance difference among females, which is also reflected in the αSyn within the microglia. (Fang, Espey, Yu, Agirman, & Hsiao, in preparation for publication). To assess if prodromal intestinal inflammation exacerbates the onset of PD-related neuroinflammation, microglia and αSyn aggregation of LRRK2 G2019S mice were assessed at an earlier time point of 23 weeks old rather than 52 weeks old. Microglia with a positive αSyn signal were manually counted to examine any differences of neuroinflammation and αSyn aggregation in water- or DSS-treated LRRK2 G2019S mice **(Fig. 5a-5c)**. There were no differences in the amount of microglia or the αSyn-positive microglia between water- and DSS-treated LRRK2 G2019S mice, revealing that at a younger age, there is no difference in the overall amount of microglia recruited or the amount of microglia that uptake αSyn.

To assess αSyn accumulation in the SN, mean fluorescent intensity (MFI) was utilized, where a more intense fluorescent signal represents an increase in αSyn aggregations **(Fig. 5d-5f)**. Within the entire SN area, there were no differences in MFI in water- or DSS-treated LRRK2 G2019S mice, indicating that the overall amount of αSyn aggregations present in the SN had no difference **(Fig. 5e, 5f)**. Interestingly, when αSyn MFI was assessed for a positive signal only within the microglial IBA-1 signal, DSS-treated males showed increased intensity compared to water-treated males **(Fig. 5a, 5d)**. This data suggests that while overall αSyn accumulation in the SN is not different, males afflicted with DSS colitis uptake more αSyn in their microglia compared to their water treated cohort.

By examining αSyn accumulation in a younger mouse model, we analyzed if αSyn would be the factor that mediated observed brain pathology in the late time point. We saw that prodromal intestinal inflammation exacerbates αSyn uptake in a male but not female LRRK2 G2019S DSS-colitis model but does not affect overall amounts of microglia or the amount of microglia that uptake αSyn.

Discussion

The major finding of this study supports the notion that the Parkinson's disease (PD)-causing LRRK2 G2019S mutation i) increases susceptibility to intestinal inflammation and that ii) early chronic gut inflammation exacerbates and accelerates neurodegeneration, and possibly expedites PD neuroinflammation. While the link between PD and inflammatory bowel disease (IBD) has been shown through prodromal gastrointestinal symptoms in PD patients, the LRRK2 G2019S mutation, and previous PD mouse model studies, the questions of how these two diverse organ systems are physiologically linked, and how gut inflammation may directly affect the brain, remain.

The answer may lie in the widely developing field of gut-brain cross talk. Indeed, many prodromal non-motor symptoms of PD involve the gastrointestinal system, and our results support that the gut and the brain are in communication. Hallmark PD neuropathology includes intraneuronal accumulations of alpha-synuclein (αSyn) aggregations, and previous studies have found that these accumulations are also found in the gastrointestinal tract of PD patients (Beach, et al., 2016; Braak, de Vos, Bohl, & Tredici, 2006; Shannon, et al., 2012). One hypothesis, commonly referred to as the Braak hypothesis, proposes that αSyn present in the gastrointestinal tract travels from the enteric to the central nervous system via the vagus nerve, where it selectively destroys dopaminergic neurons in the SN (Herrera, Castaño, Venero, & Machado, 2000; Braak, de Vos, Bohl, & Tredici, 2006; Svensson, et al., 2015; Chandra, Hiniker, Kuo, Nussbaum, & Liddle, 2017; Kim, et al., 2019; Kuo, et al., 2010). Findings that support this hypothesis demonstrate that αSyn misfolding and aggregation may begin in the gut and propagate to the brain, resulting in PD-neuropathology. Other studies find that the Braak hypothesis may only be true for certain types of PD, such as patients with a young onset and long duration of motor symptoms, but the vast majority (an estimated 80-100%) fit the Braak staging scheme (Jellinger, 2019).

While the exact mechanism of αSyn exchange is unknown, one compelling idea involves the gut microbiome's interaction with the enteric nervous system. Dysbiosis in the gut microbiome has been seen in human patients afflicted with PD, suggesting the gut's role in the disease and its phenotype (Scheperjans, et al., 2015; Unger, et al., 2016). In a mouse PD-mouse model overexpressing αSyn, gut microbes were found to promote αSyn-mediated motor deficits and brain pathology (Sampson, et al., 2016), indicating metabolites may play a causal role. Popular contenders include short chain fatty acids (SCFAs), one of the main metabolite products of the gut microbiome (Sanna, et al., 2019). They can exert neuroprotective effects in the central nervous system (CNS) by upregulating neurotrophic factors (Wu, et al., 2008), and they were found to be essential for mouse microglial function (Erny, et al., 2015). Furthermore, in different mouse PD models, different types of SCFA demonstrated a protective effect against dopaminergic neurodegeneration in the SN. Coupled with the finding that SCFAs are commonly found to be reduced in fecal samples of PD patients (Unger, et al., 2016), SCFAs may be a major metabolite from the gut that affects PD neuropathology in gut-brain crosstalk.

In our data, decreased dopaminergic neurons in a PD mouse model afflicted with DSS-induced gut inflammation is a consistent finding (Grathwohl, et al., 2021). However, rather than an artificially occurring PD model such as the αSyn Tg mouse, our mouse model utilizes a PD pathogenesis that is naturally developing and based on the human genetic mutation in LRRK2, which exhibits high face and construct validity for PD.

We assessed brain pathology at an earlier time point to assess the potential for DSS to expedite, in addition to exacerbate, the onset of PD neuropathology. Most other studies use mouse models aged 65 weeks or older to show neurodegeneration (Xiong, et al., 2018; Grathwohl, et al., 2021), whereas our mouse model is 52 weeks old. We chose this age due to our colleague's finding that PD-related motor deficits were exacerbated in DSS-treated LRRK2 G2019S males by 52 weeks old (Fang, Espey, Yu, Agirman, & Hsiao, in preparation for publication).

We show significant neurodegeneration in DSS-treated LRRK2 G2019S mice aged 52 weeks, demonstrating the effect of gut inflammation on expediting the onset of PD neuropathology. This is confirmed by our data showing no significant difference in dopaminergic neuron loss between water treated WT and LRRK2 G2019S mice, which is too early a time point for natural development of neurodegeneration without DSS-induced gut inflammation. We demonstrate that the influence of prodromal intestinal inflammation not only exacerbates dopaminergic neurodegeneration of the SN, but also accelerates the onset of PD-related neurodegeneration driven by the LRRK2 G2019S mutation.

In addition to neurodegeneration, we found exacerbated PD-related neuroinflammation by DSS colitis at 52 weeks old. Other studies have not examined for neuroinflammatory markers of PD models undergoing gut inflammation specifically in the SN, the brain region where αSyn aggregations are known to occur in PD, although studies have found increased neuroinflammatory markers in other regions of the mouse brain with DSS colitis (Carloni, et al., 2021). Our results show increased microglial activation, lysosomal formation, and lysosomal-positive microglia within the SN of DSS-treated LRRK2 G2019S mice, indicating increased neuroinflammation in the SN that was exacerbated by DSS colitis.

Autophagy in the brain utilizes lysosomes, along with other cellular mechanisms, to clear αSyn aggregates. Autophagy and lysosome dysfunctions are known in PD (Tanji, Mori, Kakita, Takahashi, & Wakabayashi, 2011). Our results show that mice with DSS-colitis have an increase in lysosomal formation, however, this does not indicate the efficacy of lysosomal αSyn clearance. Previous studies have shown that the LRRK2 G2019S mutation demonstrate a PD-like neuropathology through αSyn accumulations and defects in lysosomal activity in cell lines (Obergasteiger, et al., 2020; Hu, et al., 2018) as well as defects in autophagy in PD patients with the LRRK2 G2019S mutation (Hui, et al., 2018). With decreased lysosomal activity shown in cell lines (Obergasteiger, et al., 2020), perhaps the lysosomes are present but ineffective at

clearing αSyn aggregates. Further analysis on αSyn aggregates present in the SN will need to be assessed (Fang, Espey, Yu, Agirman, & Hsiao, in preparation for publication).

The sex difference in our study demonstrates that 52-week-old male LRRK2 G2019S mice with DSS colitis had more severe neurodegeneration compared to male WT mice with DSS colitis. When combined with our colleague's behavioral data that PD-related motor deficits were exacerbated in DSS-treated LRRK2 G2019S males (Fang, Espey, Yu, Agirman, & Hsiao, in preparation for publication), we show that DSS-induced gut inflammation affects the male PD-model more severely by 52 weeks of age. Incidence of PD in patients is twice as high in males than females, (Gillies, Pienaar, Vohra, & Qamhawi, 2014), and our data demonstrates an increased risk in males as well. We did not observe sex differences in response to DSS-induced gut inflammation; some studies found a higher incidence of IBD among females (Nguyen, Chong, & Chong, 2014), while others found no sex differences (Dahlhamer, Zammitti, Ward, Wheaton, & Croft, 2015). Some of our data may seem to demonstrate trending differences between males and females, but because of the vast physiological differences between sexes, it is not appropriate to cross-compare these data (McCarthy & Arnold, 2011). To do so, a mouse model such as the Four Core Genotypes Model should be utilized (Arnold & Chen, 2009).

Our PD mouse model shows no significant difference of neuroinflammation at 23 weeks old, indicating this time point is too early to see PD-related increases in microglia or microglia that uptake αSyn. However, and remarkably, 23-week-old males show an increase in αSyn load per microglia. This may indicate that microglia are receiving αSyn from a source outside the SN, or perhaps αSyn aggregates are more concentrated within the microglia than outside the microglia in males due to defects in αSyn clearance. Considering our findings that males are more severely affected by the PD phenotype when afflicted with gut inflammation, and our findings that αSyn per microglia and within the SN is increased in male DSS-treated 52-week-old mice as well, perhaps the onset of pathogenic αSyn accumulation occurs by 23 weeks in males with DSS colitis. Further exploration should include assessments of dopaminergic

neurodegeneration and αSyn accumulation in the colon and enteric neurons to assess the effects of prodromal intestinal inflammation on the onset of neuroinflammation and neurodegeneration.

One question that arises is whether increased chronic DSS severity itself induces more severe neuropathology that was observed in our study. Because of our finding that DSS-treated WT mice show no significant TH-positive neuron loss in the SN at 52 weeks old, it is likely that early life gut inflammation alone does not induce PD-like pathology. To address the effects of severe gut inflammation on neuropathology, a DSS titration should be administered in WT and LRRK2 G2019S mice to determine if elevated severity of DSS colitis can sufficiently induce neuropathology.

In summary, we show that modeling prodromal gut inflammation exacerbates and expediates neurodegeneration, as well as promotes neuroinflammation, in the LRRK2 G2019S mouse model. We demonstrate that male LRRK2 G2019S mice with prodromal gut inflammation have increased αSyn aggregates in their microglia, indicating that pathological αSyn aggregations may occur in response to prodromal symptoms. These results show a clear gut-brain communication that involves the ability of early gut inflammation to worsen PD neuropathology in genetically predisposed mice. These results may inform further research on gut-brain and neuroimmune contributions to human PD, as well as other neurodegenerative diseases such as Alzheimer's disease or amyotrophic lateral sclerosis.
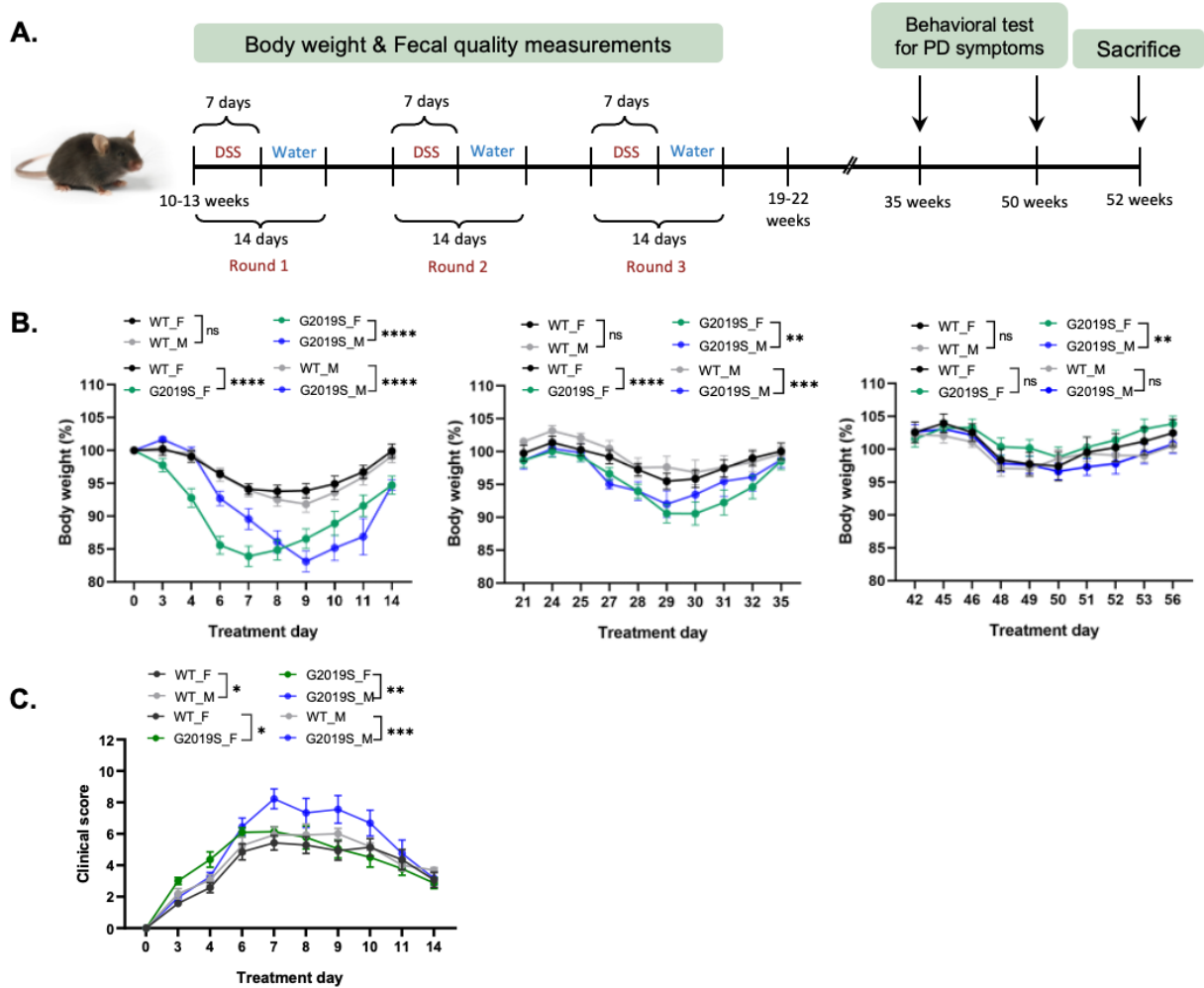
Figures

Figure 1: Experimental colitis timeline and body weight results of male and female LRRK2 G2019S and WT mice. | **A.** 10–13-week-old male and female LRRK2 G2019S and WT mice underwent three rounds of 2% dextran sulfate sodium (DSS) treatment to induce chronic gut inflammation, during which body weight and fecal quality measurements were taken to assess severity of gut inflammation. PD-related motor deficits were observed through behavior tests at 35 and 50 weeks old and reported in a colleague's work (Fang, Espey, Yu, Agirman, & Hsiao, in preparation for publication). Mice were sacrificed at 52 weeks old, and brains collected for substantia nigra (SN) visualization for PD-related neurodegeneration and neuroinflammation analysis. **B.** Body weight measurement throughout the three rounds of DSS treatment of male and female LRRK2 G2019S and WT mice. **C.** Clinical score during acute DSS-induced intestinal inflammation, where a higher score represents more severe symptoms. | Two-way ANOVA was utilized for multiple group comparisons. All data are represented as mean ± s.e.m. (standard error of the mean). *P < 0.05 was considered statistically significant.
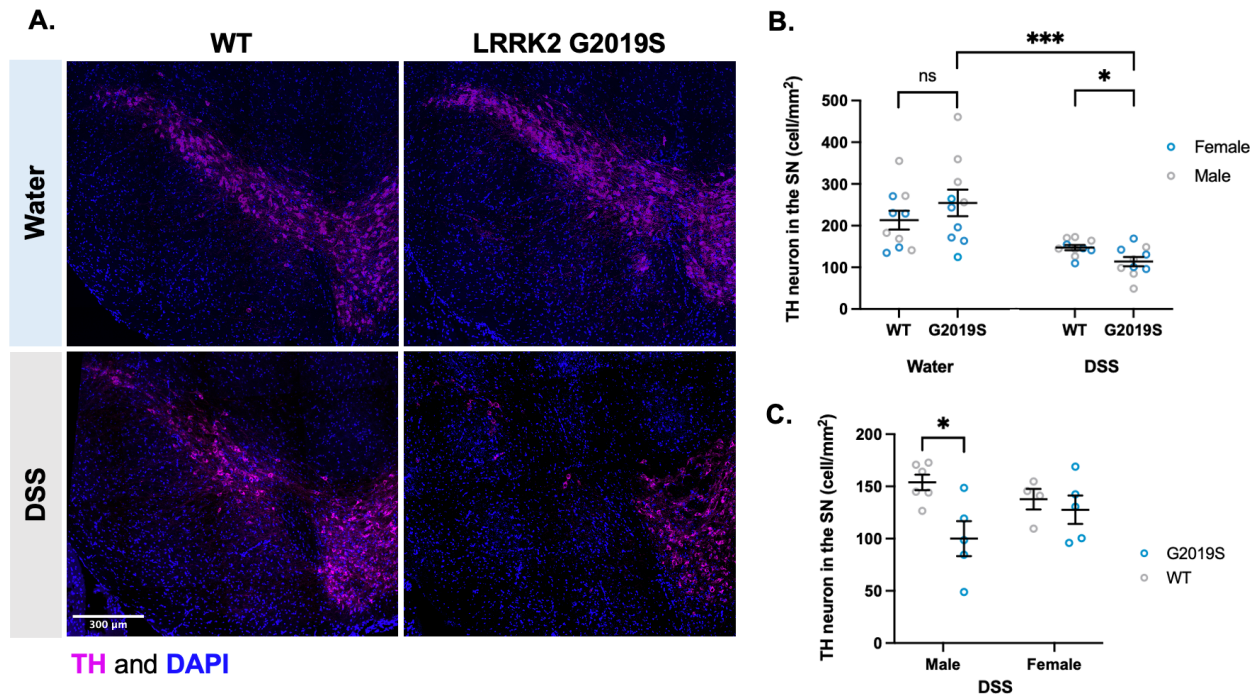
Figure 2: Decreased TH-positive neurons in SN of DSS-treated LRRK2 G2019S mice aged 52 weeks. | **A.** Representative images of SN of water- and DSS- treated WT and LRRK2 G2019S mice. Magenta represents tyrosine hydroxylase (TH)-positive neurons, and blue represents DAPI stained nuclei. Scale bar =300 µm. **B.** Manual quantification of TH-positive neuronal density in the SN of water- and DSS-treated WT and LRRK2 G2019S mice per SN area. Two-way ANOVA demonstrated significance of interaction of treatment and genotype ($F_{(1,36)}$ =3.321, P =0.0767) (Treatment ($F_{(1,36)}$ =25.18, P <0.0001), Genotype ($F_{(1,36)}$ =0.03564, P =0.8513)). P-values were determined by Tukey's post hoc test (*P <0.05, ***P <0.0001, ns =0.066). **C.** Manual quantification of TH-positive neuronal density in SN of DSS-treated male and female LRRK2 G2019S and WT mice per SN area. Significance of genotype and sex was determined by two-way ANOVA ($F_{(1,16}$ =3.108, P =0.0970) (Genotype ($F_{(1,36)}$ =6.641, P =0.0203), Sex ($F_{(1,36)}$ =0.2158, P =0.06485)) followed by Tukey's post hoc test (*P <0.05). | All water-treated groups, n =5. DSS-treated LRRK2 G2019S male and female, n =5. DSS-treated WT females, n =4. DSS-treated WT males, n =6. All data are represented as mean ± s.e.m. (standard error of the mean).
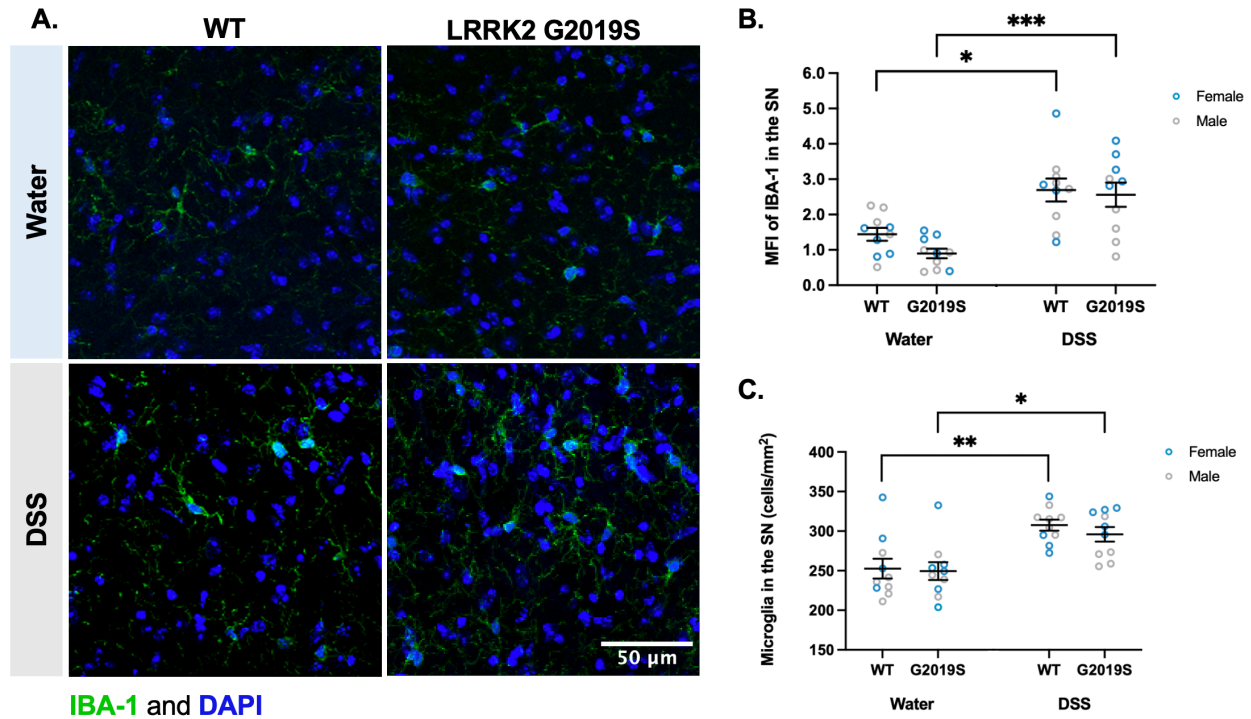
Figure 3: Increased IBA-1 mean fluorescent intensity (MFI) in SN of DSS-treated WT and LRRK2 G2019S mice aged 52 weeks. | **A.** Representative images within SN of water- and DSS- treated WT and LRRK2 G2019S mice. Green represents IBA-1-stained microglia, and blue represents DAPI-stained nuclei. Scale bar =50 μm. **B.** MFI of IBA1 in the SN of water- and DSS- treated WT and LRRK2 G2019S mice. Two-way ANOVA determined significance of interaction of treatment and genotype $(F_{(1,36)}=0.6125, P =0.4390)$ (Treatment $(F_{(1,36)} =30.88, P <0.0001)$, Genotype $(F_{(1,36)} =1.672, P =0.2042)$) followed by Tukey's post hoc test (*P <0.05, ***P <0.0001). **C.** Manual quantification of microglia per SN area. Significance of interaction of treatment and genotype was determined by two-way ANOVA $(F_{(1,36)} =0.1710, P =0.6817)$ (Treatment $(F_{(1,36)} =24.66, P <0.0001)$, Genotype $(F_{(1,36)} =0.5225, P =0.4745)$) followed by Tukey's post hoc test (*P <0.05, **P <0.01). | All water-treated groups, n =5. DSS-treated LRRK2 G2019S male and female, n =5. DSS-treated WT females, n =4. DSS-treated WT males, n =6.
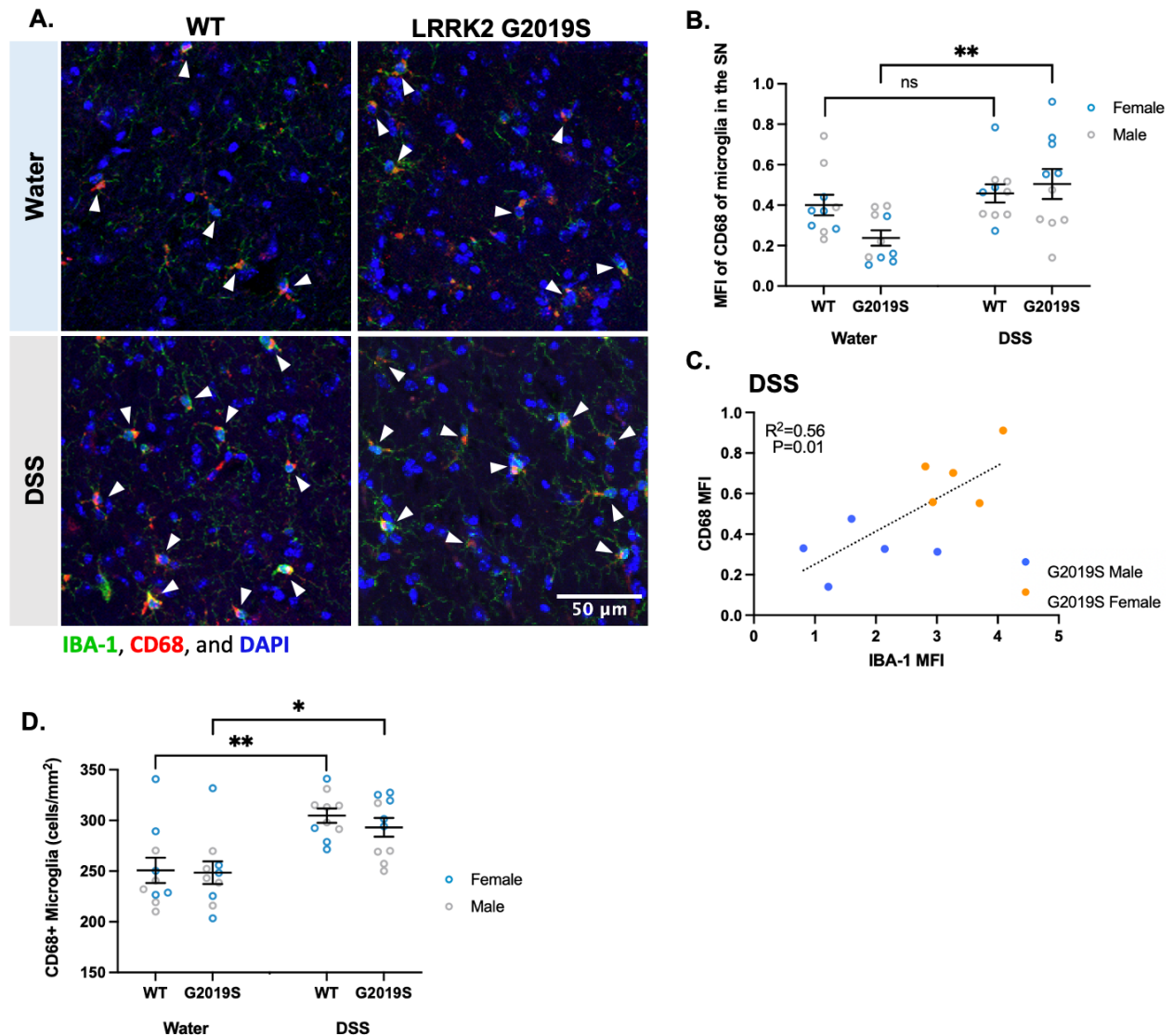
Figure 4: Increased CD68 mean fluorescent intensity (MFI) and CD68-positive microglia in SN of DSS-treated WT and LRRK2 G2019S mice aged 52 weeks. | **A.** Representative images within SN of microglia (green) and lysosomes (red). Carrots point to CD68 as puncta within the IBA-1 signal. **B.** MFI of CD68 in the SN of water- and DSS- treated WT and LRRK2 G2019S mice. Significance of interaction of treatment and genotype was determined by two-way ANOVA ($F_{(1,36)}$ =3.801, P =0.0590) (Treatment ($F_{(1,36)}$ =9.091, P <0.0047), Genotype($F_{(1,36)}$ =1.178, P =0.2849)) followed by Tukey's post hoc test (**P<0.01, ns=0.97). **C.** Correlation graph of IBA-1 and CD68 MFI of DSS-treated mice. **D.** Manual quantification of CD68-positive microglia per SN area. Two-way ANOVA determined significance of interaction of treatment and genotype ($F_{(1,36)}$=0.2019, P=0.6559) (Treatment ($F_{(1,36)}$ =23.32, P <0.0001), Genotype ($F_{(1,36)}$ =0.4635, P =0.5004)) followed by Tukey's post hoc test (*P<0.05, **P<0.01). | All water-treated groups, n=5. DSS-treated LRRK2 G2019S male and female, n = 5. DSS-treated WT females, n = 4. DSS-treated WT males, n=6.

A.

Water | DSS

αSyn, IBA-1, and DAPI

B.

ns

Microglia/area (cell/mm²)

○ DSS
○ Water

Male   Female

C.

ns

Asyn+ Microglia (%)

○ DSS
○ Water

Male   Female

D.

*

MFI of aSyn in Microglia in SN

○ DSS
○ Water

Male   Female

E.

Water | DSS

TH and αSyn

F.

ns

MFI of aSyn+ in the SN
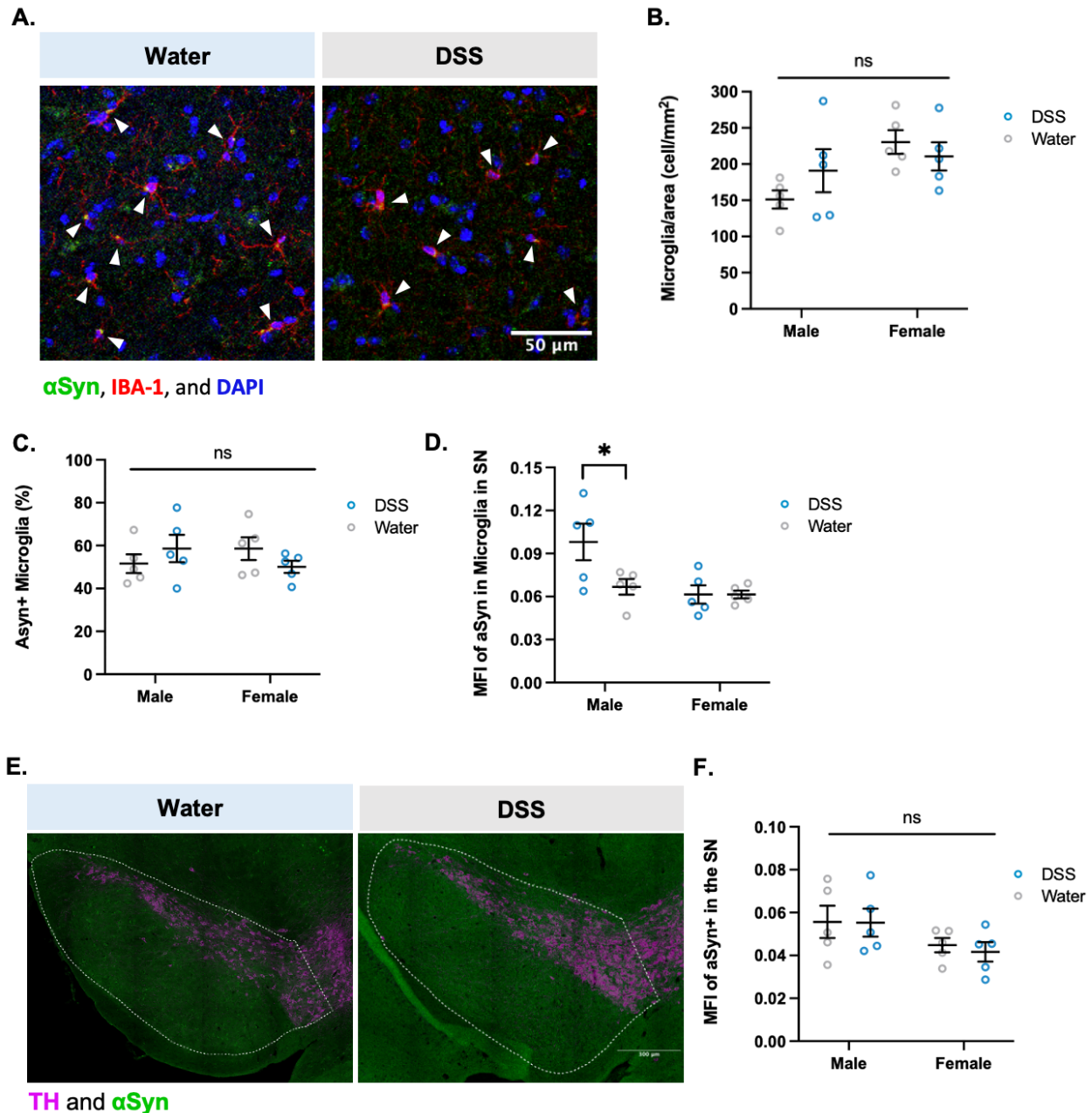
○ DSS
○ Water

Male   Female

Figure 5: DSS-treated LRRK2 G2019S males aged 23 weeks show increased αSyn uptake in microglia. | **A.** Representative images of αSyn (green) within microglia (red) in the SN area. Scale bar =50 μm. Carrots point to αSyn within the IBA-1 signal. **B.** Manual quantification of microglia per area in SN area of DSS- and water-treated male and female mice. Significance of interaction of sex and treatment was determined by two-way ANOVA ($F_{(1,16)}$ =2.105, P =0.1661) (Sex ($F_{(1,16)}$ =5.805, P =0.0284), Genotype ($F_{(1,16)}$ =0.2348, P =0.6345)) followed by Tukey's post hoc test (ns >0.05). **C.** Percent αSyn-positive microglia in SN of DSS- and water-treated male and female mice. Significance of interaction of sex and treatment was determined by two-way ANOVA ($F_{(1,16)}$ =2.509, P =0.1328) (Sex ($F_{(1,16)}$ =0.02476, P =0.8769), Genotype ($F_{(1,16)}$ =0.02057, P =0.8877)) followed by Tukey's post hoc test (ns >0.05). **D.** Mean fluorescent intensity (MFI) of αSyn only within the microglia of the SN area. Two-way ANOVA determined significance of interaction of sex and treatment ($F_{(1,16)}$=4.100, P =0.0599) (Sex ($F_{(1,16)}$ =7.340, P =0.0155), Genotype ($F_{(1,16)}$ =4.090, P =0.0602)) followed by Tukey's post hoc test (*P <0.05). **E.** Representative images of αSyn (green) within the SN (outlined) with dopaminergic neurons

21

(magenta). Scale bar =300 µm. **F.** MFI of αSyn in the entire SN area as shown in figure 5e. Significance of interaction of sex and treatment was determined by two-way ANOVA ($F_{(1,16)}$ =0.06024, P =0.8092) (Sex ($F_{(1,16)}$ =4.605, P=0.0476), Genotype ($F_{(1,16)}$ =0.09521, P =0.7616)) followed by Tukey's post hoc test (ns >0.05). | All DSS- and water-treated groups, n =5.

References

Alessi, D. R., & Sammler, E. (2018). LRRK2 kinase in Parkinson's disease: Defects in vesicular
trafficking and immune responses are found in Parkinson's disease. *Science, 360*(6384),
36-37.

Arnold, A. P., & Chen, X. (2009). What does the "four core genotypes" mouse model tell us
about sex differences in the brain and other tissues? *Frontiers in Neuroendocrinology*, 1-
9.

Beach, T. G., Corbillé, A.-G., Letournel, F., Kordower, J. H., Kremer, T., Munoz, D. G., . . .
Derkinderen, P. (2016). Multicenter Assessment of Immunohistochemical Methods for
Pathological Alpha-Synuclein in Sigmoid Colon of Autopsied Parkinson's Disease and
Control Subjects. *J Parkinsons Dis*, 761–770.

Braak, H., de Vos, R. A., Bohl, J., & Tredici, K. D. (2006). *Neuroscience*.

Carloni, Bertocchi, A., S, M., M, B., M, E., A, B., . . . M., R. (2021). Identification of a choroid
plexus vascular barrier closing during intestinal inflammation. *Science*, 439-448.

Chandra, R., Hiniker, A., Kuo, Y.-M., Nussbaum, R. L., & Liddle, R. A. (2017). α-Synuclein in gut
endocrine cells and its implications for Parkinson's disease. *JCI Insight*.

Dahlhamer, J. M., Zammitti, E. P., Ward, B. W., Wheaton, A. G., & Croft, J. B. (2015).
Prevalence of Inflammatory Bowel Disease Among Adults Aged ≥18 Years — United
States, 2015. *MMWR Morb Mortal Wkly*, 1166-1169.

Erny, D., de Angelis, A. L., Jaitin, D., Weighofer, P., Staszewski, O., David, E., . . . Mc. (2015).
Host microbiota constantly control maturation and function of microglia in the CNS.
Nature Neuroscience, 965-977.

Fang, P., Espey, H., Yu, L., Agirman, G., & Hsiao, E. Y. (in preparation for publication). Sex
difference in prodromal intestinal inflammation promoting LRRK2G2019S mediated
symptoms of Parkinson's disease.

Gillies, G. E., Pienaar, I. S., Vohra, S., & Qamhawi, Z. (2014). Sex differences in Parkinson's disease. *Frontiers in Neuroendocrinology*, 370-384.

Grathwohl, S., Quansah, E., Maroof, N., Steiner, J. A., Spycher, L., Benmansour, F., . . . Selhausen, M. (2021). Specific immune modulation of experimental colitis drives enteric alpha-synuclein accumulation and triggers age-related Parkinson-like brain pathology. *Free Neuropathology*.

Herrera, A., Castaño, A., Venero, J., & Machado, C. A. (2000). The Single Intranigral Injection of LPS as a New Model for Studying the Selective Effects of Inflammatory Reactions on Dopaminergic System. *Neurobiology of Disease*, 429-447.

Hu, D., Niu, J.-y., Xiong, J., Nie, S.-k., Zeng, F., & Zhang, Z.-h. (2018). LRRK2 G2019S Mutation Inhibits Degradation of α-Synuclein in an In Vitro Model of Parkinson's Disease. *Current Medical Science*, 1012-1017.

Hui, K. Y., Fernandez-Hernandez, H., Hu, J., Schaffner, A., Pankratz, N., Hsu, N.-Y., . . . Haritunia. (2018). Functional Variants in LRRK2 Confer Pleiotropic Effects on Risk for Crohn's Disease and Parkinson's Disease. *Science Translational Medicine*.

Jellinger, K. A. (2019). Is Braak staging valid for all types of Parkinson's disease? *Journal of Neural Transmission*, 423-431.

Kim, S., Kwon, S.-H., Kam, T.-I., Panicker, N., Karuppagounder, S. S., Lee, S., . . . Lee, G. (2019). Transneuronal Propagation of Pathologic α-Synuclein from the Gut to the Brain Models Parkinson's Disease Author links open overlay panel. *Neuron*, 627-641.

Kuo, Y.-M., Li, Z., Jiao, Y., Gaborit, N., Pani, A. K., Orrison, B. M., . . . Nussbaum, R. L. (2010). Extensive enteric nervous system abnormalities in mice transgenic for artificial chromosomes containing Parkinson disease-associated α-synuclein gene mutations precede central nervous system changes. *Human Molecular Genetics*, 1633-1650.

Lee, H.-S., Lobbestael, E., Vermeire, S., Sabino, J., & Cleynen, I. (2021). Inflammatory bowel disease and Parkinson's disease: common pathophysiological links. *BMJ Gut*.

Marras, C., Beck, J., Bower, J., Roberts, E., Ritz, B., Ross, G. W., . . . Tanner, C. (2018).

      Prevalence of Parkinson's disease across North America. *npj Parkinson's Disease*.

McCarthy, M. M., & Arnold, A. P. (2011). Reframing sexual differentiation of the brain . *Nature*

      Neuroscience, 677-683.

Nguyen, G. C., Chong, C. A., & Chong, R. Y. (2014). National estimates of the burden of

      inflammatory bowel disease among racial and ethnic groups in the United States.

      Journal of Crohn's and Colitis, 288-295.

Obergasteiger, J., Frapporti, G., Lamonaca, G., Pizzi, S., Picard, A., Lavdas, A. A., . . . Corti, C.

      (2020). Kinase inhibition of G2019S-LRRK2 enhances autolysosome formation and

      function to reduce endogenous alpha-synuclein intracellular inclusions. *Cell Death*

      Discovery, 6-45.

Papathanou, M., M, C., MC, D., Z, B., S, D., H, P., . . . Å, W.-M. (2018). Targeting VGLUT2 in

      Mature Dopamine Neurons Decreases Mesoaccumbal Glutamatergic Transmission and

      Identifies a Role for Glutamate Co-release in Synaptic Plasticity by Increasing Baseline

      AMPA/NMDA Ratio. *Frontiers in Neural Circuits*.

Paul, E. J., Kalk, E., Tossell, K., Irvine, E. E., Franks, N. P., Wisden, W., . . . Ungless, M. A.

      (2018). nNOS-Expressing Neurons in the Ventral Tegmental Area and Substantia Nigra

      Pars Compacta. *eNeuro*.

Peter, I., Dubinsky, M., Bressman, S., Park, A., Lu, C., Chen, N., & Wang, A. (2018). Anti–

      Tumor Necrosis Factor Therapy and Incidence of Parkinson Disease Among Patients

      With Inflammatory Bowel Disease. *JAMANeurology*, 939-946.

Poewe, W., Seppi, K., Tanner, C., Halliday, G. M., Brundin, P., Volkmann, J., . . . Lang, A. E.

      (2017). Parkinson disease. *Nature*.

Sampson, T. R., Debelius, J. W., Thron, T., Janssen, S., Shastri, G. G., Ilhan, Z. E., . . .

      Shannon, K. M. (2016). Gut Microbiota Regulate Motor Deficits and Neuroinflammation

      in a Model of Parkinson's Disease. *Cell*, 1469-1480.

Sanna, S., van Zuydam, N. R., Mahajan, A., Kurlishikov, A., Vila, A. V., Võsa, U., . . . Fu. (2019).

 Causal relationships among the gut microbiome, short-chain fatty acids and metabolic

 diseases. *Nature Genetics*, 600-605.

Scheperjans, F., Aho, V., Pereira, P. A., Koshkinen, K., Paulin, L., Pekkonen, E., . . . Auvinen,

 P. (2015). Gut microbiota are related to Parkinson's disease and clinical phenotype.

 Movement Disorders, 350-358.

Shannon, K. M., Keshavarzian, A., Mutlu, E., Dodiya, H. B., Daian, D., Jaglin, J. A., & Kordower,

 J. H. (2012). Alpha-synuclein in colonic submucosa in early untreated Parkinson's

 disease. *Movement Disorders*, 709-715.

Svensson, E., Horváth-Puhó, E., Thomsen, R. W., Djurhuus, J. C., Pedersen, L., Borghammer,

 P., & Sørensen, H. T. (2015). Vagotomy and subsequent risk of Parkinson's disease.

 Annals of Neurology, 522-529.

Takagawa, T., Kitani, A., Fuss, I., Levine, B., Brant, S. R., Peter, I., . . . Stober, W. (2018). An

 increase in LRRK2 suppresses autophagy and enhances Dectin-1–induced immunity in

 a mouse model of colitis. *Science Translational Medicine*.

Tanji, K., Mori, F., Kakita, A., Takahashi, H., & Wakabayashi, K. (2011). Alteration of

 autophagosomal proteins (LC3, GABARAP and GATE-16) in Lewy body disease.

 Neurobiology of Disease, 690-697.

Thompson, L., Barraud, P., Andersson, E., Kirik, D., & Björklund, A. (2005). Identification of

 Dopaminergic Neurons of Nigral and Ventral Tegmental Area Subtypes in Grafts of Fetal

 Ventral Mesencephalon Based on Cell Morphology, Protein Expression, and Efferent

 Projections. *The Journal of Neuroscience*.

Unger, M., Spiegel, J., Dillmann, K.-U., Grundmann, D., Philippeit, H., Bürmann, J., . . . Schäfer,

 K.-H. (2016). Short chain fatty acids and gut microbiota differ between patients with

 Parkinson's disease and age-matched controls. *Parkinsonism & Related Disorders*, 66-

 72.

Van Den Eeden, S. K., Tanner, C. M., Bernstein, A. L., Fross, R. D., Leimpeter, A., Bloch, D. A.,

    & Nelson, L. M. (2003). Incidence of Parkinson's Disease: Variation by Age, Gender,

    and Race/Ethnicity. *American Journal of Epidemiology*.

Villumsen, M., Aznar, S., Pakkenberg, B., Jess, T., & Brudek, T. (2019). Inflammatory bowel

    disease increases the risk of Parkinson's disease: a Danish nationwide cohort study

    1977–2014. *BMJ Gut*, 18-24.

Weimers, P., Halvarsaon, J., Saudners-Pullman, R., Ludvigsson, J., Peter, I., Olén, O., &

    Burisch, J. (2016). Inflammatory Bowel Disease and Parkinson's Disease: A Reply to

    Letter to the Editor of Shih-Wei Lai. *Inflammatory Bowel Diseases*, e127.

Wirtz, S., Popp, V., Kindermann, M., Gerlach, K., Weigmann, B., Fichtner-Feigl, S., & Neurath,

    M. F. (2017). Chemically induced mouse models of acute and chronic intestinal

    inflammation. *Nature Protocols*, 1295-1309.

Wu, X., Chen, P. S., Dallas, S., Wilson, B., Block, M. L., Ang, C.-C., . . . Hong, J.-S. (2008).

    Histone deacetylase inhibitors up-regulate astrocyte GDNF and BDNF gene transcription

    and protect dopaminergic neurons. *International Journal of Neuropsychopharmacology*,

    1123-1134.

Xiong, Y., Neifert, S., Karuppagounder, S. S., Liu, Q., Stankowski, J., Lee, B. D., . . . Tessar.

    (2018). Robust kinase- and age-dependent dopaminergic and norepinephrine

    neurodegeneration in LRRK2 G2019S transgenic mice. *Proceedings of the National*

    Academy of Sciences of the U S A, 1635-1640.